

Observation of period multiplication and instability in a dc glow discharge

R. B. Wilson IV and N. K. Podder

Department of Math and Physics, Troy University, Troy, Alabama 36082, USA

(Received 24 July 2007; revised manuscript received 24 September 2007; published 25 October 2007)

The temporal dynamics in the fluctuations of the plasma floating potentials from an undriven dc glow discharge argon plasma at an intermediate gas pressure of 250 mTorr and at the range of discharge currents $I=6-50$ mA are investigated. In this study, the discharge current I is used as the plasma system's bifurcation parameter in analogy with the parameter space of a numerical dynamical system. Over several regions of the discharge current, the floating potential fluctuation time series data has been indicative of random noise, periodic oscillations, and irregular fluctuations. As the bifurcation parameter (discharge current) is increased, the Fourier spectrum of the data shows increased signs of period multiplication, quasiperiodicity, and instabilities. In addition, the computations of the correlation dimension provide some insight into the complex nature of the instabilities in the glow discharge plasma.

DOI: [10.1103/PhysRevE.76.046405](https://doi.org/10.1103/PhysRevE.76.046405)

PACS number(s): 52.25.Gj, 52.35.Fp, 52.80.Hc

I. INTRODUCTION

Nonlinear phenomena are observed in a large number of dynamical systems [1]. An important element of these systems is the appearance of deterministic chaos [1,2]. Among fluid systems, gas discharges and plasmas are very rich in dynamical behaviors due to their inherent striations, oscillations, waves, etc. Among classical plasma systems, hot filament discharges [3,4], dc glow discharge plasmas [5–8], and hollow cathode discharges [9,10] have been widely used to study chaos and instabilities because they are relatively simple to construct and operate. For a suitable set of operating conditions (plasma and floating potentials, discharge currents, ion and electron saturation currents, gas pressures, circuit impedance, etc.), various oscillations and instabilities can be introduced in these plasma discharge systems. These systems' transition to chaos has been observed through (i) period multiplication [11–18], (ii) quasiperiodicity [19–21], and (iii) intermittency [22–25].

Thanks to the mathematical tools developed in the past few decades by the pioneers of nonlinear dynamical systems, the behaviors of complex physical systems have been able to be more thoroughly understood through time delay embedding techniques [26,27]. A simple system can be constructed with easily “tunable” parameters such as driving discharge current or gas pressure. In this way, the study of fluctuations in experimental systems can be carried out using essentially the same techniques that have been used on numerical systems, which have yielded so many beautiful results in the field of nonlinear dynamical systems [1]. More precisely, making scalar measurements on an experimental system and generating a time series can yield insight into the existence of attractors and the parameter-dependent transitions within the system's behavior [26–29]. By these means, researchers have the ability to undertake a more global understanding of their experimental systems by considering patterns of behavior change throughout the system's parameter space.

Previously, nonlinear investigations into the period-multiplication transition to chaos have considered a variety of measurable fluctuating aspects: (i) in the hot filament discharges, which include floating potentials [11], plasma po-

tentials [12,14], and plasma currents [13] and (ii) in the glow discharge plasmas, which include electrostatic potentials [16], plasma current and voltage [17], and current density [18]. Incredibly, the particular observable quantities used in these plasma systems seem to have become almost detail, as the results of such investigations have been so remarkably similar.

In the past, experimental investigations on plasma systems have shown the occurrence of different transitions to chaos and instability [11–25]. This is commonly done by reporting three time series for three different values of the bifurcation parameter, with one time series in a stable mode, one in the transition state, and a final time series exhibiting chaotic dynamics. Depending on the kind of transition to chaos exhibited by the system, this is an efficient and simple way to show the existence of the transition, and, more importantly, the possible existence of chaotic behavior in the system. This is an important type of investigation, a logical extension of which is a higher-resolution exploration into the behavior of the experimental system with respect to a “bifurcation parameter” [12,30].

The goal of this paper is to study the instabilities in the floating potentials from a dc glow discharge plasma by a more precise control of its bifurcation parameter, i.e., the glow discharge plasma current. Specifically, the plasma floating potential fluctuations are measured with a fixed 1-mA incremental step of the discharge current. The bifurcation scheme of the numerical analog (the logistic map as an example) is first presented and later compared with the experimental glow discharge plasma system. The similarities among the argon glow discharge system's bifurcation diagram obtained in this study, and the ones reported earlier in a hot filament discharge by Greiner *et al.* and in neon glow discharge by Atipo *et al.*, indicate a universal behavior in both types of plasma discharges.

II. PERIOD MULTIPLICITY IN NUMERICAL SYSTEMS

Our motivation behind this work traces back to the observation of the well-known behavior of the logistic map [2,31,32]. One of the most studied numerical systems is the

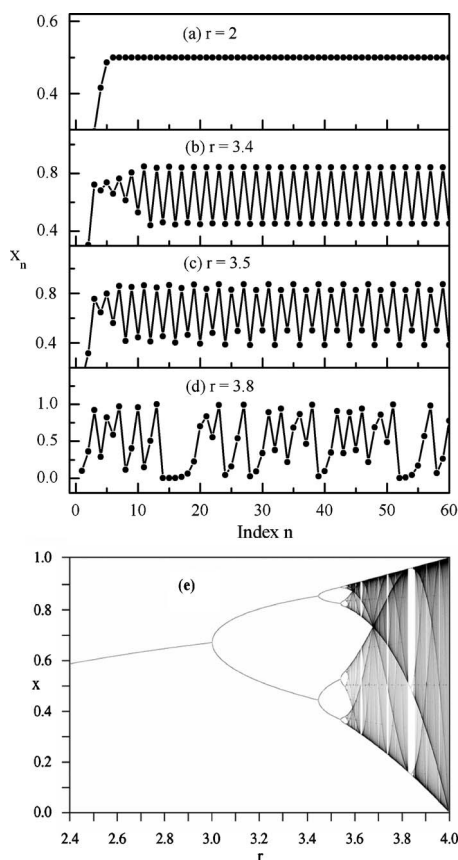


FIG. 1. Logistic map iterations. (a) For an r value of 2, the iterations of the map converge to a single value, (b) for $r=3.4 > \lambda_1$, the iterations fall into a perfectly periodic fluctuation of two values (period 2), (c) for $r=3.5 > \lambda_2$, the iteration fluctuation doubles its period to 4, (d) for $r=3.8 > \lambda_c$, the fluctuation loses stability, entering a chaotic state, and (e) the bifurcation diagram for the logistic map in the parameter r space (taken from the Wikipedia website in Ref. [32]).

logistic map $x_{n+1} = rx_n(1-x_n)$, where $n=0, 1, 2, 3, \dots, x_n$ assumes a value between 0 and 1, and r is a real-valued parameter. The plot of x_n versus n generated using $x_0=0.1$ is shown in Fig. 1. The sequence generated by iterating this map converges to a fixed point for low values of the parameter r , e.g., $r=2$, and can be seen in Fig. 1(a). There exists an r value called a first bifurcation point $r=\lambda_1$ beyond which the behavior becomes a stable two-cycle or single-frequency periodic behavior which is seen in Fig. 1(b), forever alternating between two values. This is the case until a second bifurcation point $r=\lambda_2$, where the behavior of the sequence then doubles its period into a four-cycle, which is seen Fig. 1(c). This pattern continues as r is increased, passing many bifurcation points, doubling the period each time until at a critical value $r=\lambda_c$, where the behavior of the iterated map loses stability, becoming chaotic as shown in Fig. 1(d). This process is known as the period doubling route to chaos.

The bifurcation diagram for the logistic map is taken from the Wikipedia website [32] whose material's copyright is released into the public domain, and is shown in Fig. 1(e). The vertical axis x represents the x_n values at which the system

alternates and the corresponding values of r are plotted in the horizontal axis. In this manner, we may understand the behavior of the system as dependent upon its parameter r . This parameter dependence of fluctuation modes has been observed in other numerical systems, as well as in a wide variety of physical systems [2]. The exposition of the similarities of these behaviors and exhibition of the ubiquity of the phenomena are the driving force behind our current work. This study is an attempt to take the elegant results from modern investigations into bifurcation properties of numerical systems, and extend them into the realm of experimental dynamical systems. In particular, we wish to construct a bifurcation diagram from the fluctuation modes observed in a dc glow discharge plasma system. By taking time series measurements on the floating potential, we treat the data as though they were the numerical output of a dynamical system, and then proceed in the manner familiar to them.

III. ANALYSIS METHODS

The time series data on the glow discharge floating potential are subjected to an array of analyses, with the general goal in mind being to trace the behavior as it shifts between periodic and irregular fluctuation modes. The determination of chaos in an experimental system entails many difficulties, as pointed out very well by Kantz and Schreiber [33]. The aim of this study is not directly to examine in detail any chaotic structure in the system, but merely to point out the regions of stability and instability, and their structures as the bifurcation parameter changes. In order to characterize the oscillations and the regions of instability seen in the floating potential fluctuations, several analysis techniques are used and described below.

A. Fourier analysis

A time series measurement was taken of the floating potential was initially examined using a standard discrete Fourier transform [33] in order to locate any dominant frequencies inherent in the data. When present, these frequencies were recorded for the sake of monitoring the evolution of the system bifurcation. Peak frequencies were counted from the power spectrum only when the amplitude of the frequency exceeded ten times that of the average baseline noise level. This was the standard set for the distinction between noise and signal in the frequency domain. It is pointed out by Schuster [2] that “external noise can destroy the fine structure of the power spectrum.” We sought here only to record the distinguishable frequencies, in order to construct a rough bifurcation diagram.

B. Correlation dimension

The time series $\{x_1, x_2, x_3, \dots, x_N\}$ is projected into an m -dimensional attractor space by the method of delay coordinate reconstruction [26,33]. In this method, m -dimensional vectors (X_i) are obtained from the time series by using M number of scalar elements, and a “delay or lag index” τ to construct the vector as,

$$X_i = (x_i, x_{i+\tau}, x_{i+2\tau}, \dots, x_{i+(m-1)\tau}),$$

so that $X_i \in R^m$. By this construction, we may create a new set of higher-dimensional (embedded) data points, which we may consider an “orbit” in the embedding space. The number of embedded points which can be constructed in this way is M , and is given by $M=N-\tau m$, where N is the number of data points in the original time series. As a terminological note, if the data sampling time step is Δt , then the “time delay” is $\tau\Delta t$ [33]. This orbit is a geometric “rendition” of the attractor. A brief discussion of how τ is chosen will take place toward the end of this section, since in our study it is dependent upon the notion of the correlation sum, and is discussed below.

Once the time series is embedded, there are many statistics which may be implemented to yield information about the dynamics of the system being measured. In this particular study, we computed the correlation sum of the individual time series taken. This has been a widely used method for characterizing time series by distinguishing chaotic behavior from random or periodic behavior. The correlation dimension is a statistic introduced by Grassberger and Procaccia [34], which is computed on an embedded time series. One must first compute the correlation sum,

$$C(r) = \frac{1}{M^2} \sum_{i=1}^M \sum_{j \neq i}^M \Theta(r - \|X_i - X_j\|)$$

for a fixed embedding dimension m . It is a function of the neighborhood radius r , for M embedded points. This correlation sum is a normalized count of neighbors in the neighborhood of a given embedded reference point. For a properly embedded time series [34], the sum computed across the increasing value of r will tend to show some power law scaling, determined by the structure of the reconstructed attractor. The computation across r is then made for an increasing value of the embedding dimension [35]. As the embedding dimension is increased, the slope of a linear region in a log-log plot of this array of the correlation sums will converge to a single slope value, or diverge. Commonly, $d\{\log_{10}[C(r)]\}/d\{\log_{10}(r)\}$ is examined, as any linear region in $\log_{10}[C(r)]$ will show up as a plateau in the derivative. In the convergent case, the convergent slope value is interpreted as the correlation dimension.

According to Ref. [34], when the correlation integrals are computed using random noise, the slopes will increase indefinitely as the embedding dimension is increased. They go on to state that, if the statistic is applied to embedded data which lie on a strange attractor, then the slopes will reach a particular value, after which they cease to increase with embedding dimension. However, there are other claims made on experimental systems based on this statistic in Ref. [34] that a noninteger value of the correlation dimension implies chaotic dynamics [36,37] which is not stated in Ref. [34]. Furthermore, it has been shown that strange (non-integer-dimension) nonchaotic attractors can exist in numerical models in the presence of noise [38] as well as in a glow discharge plasma [39]. It is clear that the strangeness of an attractor is not a sufficient condition by which to determine

chaos in a system. In this study, we will not attempt to characterize chaos by the correlation dimension alone. The statistic may be used as an estimate for the dimensionality of the attractor of the system, if the statistic yields a finite value. This allows some insight into the geometry of the attractor.

C. Time delay

There arise many difficulties in implementing the time delay methods [40–42] on experimental data. Of the most widely addressed is the question of picking a “good” time delay. There are no embedding theorems which concern this aspect of delay embedding, since the theoretical data sets are assumed to be noise-free and infinite, thus rendering the non-zero delay value arbitrary. This creates original problems for each experimental researcher who is working with finite, noisy data. This problem has been addressed by many authors [33,41,42]. It was common for some time to use the autocorrelation function of a time series to determine the delay, by either finding the first zero, or finding the point where the function decays down to $1/e$ of its initial value [33]. But it has been shown by Fraser and Swinney [41] that using the autocorrelation is inappropriate for nonlinear systems, as it is a linear statistic. It has been suggested to use the first zero of the mutual information [41]. Though this also has become popular, it is computationally laborious.

For this study, we used the C - C algorithm of Kim *et al.* [42]. This algorithm deals with the properties of $S(m, N, r, \tau) = C(m, N, r, \tau) - C^m(1, N, r, \tau)$ over a range of delay index τ , where $C(m, N, r, \tau)$ is the m -dimensional correlation sum with fixed neighborhood radius r , and $C^m(1, N, r, \tau)$ is the one-dimensional correlation sum raised to the m th power. The computation is repeated for a small variety of values of r . This statistic is based on the notion that if the embedded points are independently and identically distributed (a good embedding), then $C(m, N, r, \tau)$ and $C^m(1, N, r, \tau)$ are equal for all m and r . Thus, by computing their difference $S(m, N, r, \tau)$ for multiple values of m , r , and for a range of τ , the first zero crossing and areas with the least variation with r will indicate a range of delay which gives an optimum distribution of embedded points in R^m .

In this way, Kim *et al.* [42] interpret the statistic $C(m, N, r, \tau)$ as the serial correlation of a nonlinear time series, and regard this as a dimensionless measure of nonlinear dependence, i.e., for fixed m , N , and r values, the plot of this statistic vs delay index is a nonlinear analog of the autocorrelation function vs delay index. This method yields an approximate range for the time delay, which is acceptable, since the embedding remains largely unaffected by small shifts in the delay quantity (assuming that the system has been appropriately sampled). Not only has it been shown to be rather robust in its applicability, yet computationally simple. In this work, several graphs, as a representative of the typical C - C computations using the experimental data, are shown in Fig. 2 for embedding dimension $m=2, 3, 4$, and 5. This particular set is generated using the time series data (fluctuations in plasma floating potential) from a glow discharge in argon at a gas pressure of 250 mTorr and discharge current $I=15$ mA. The zero crossings and delay values of

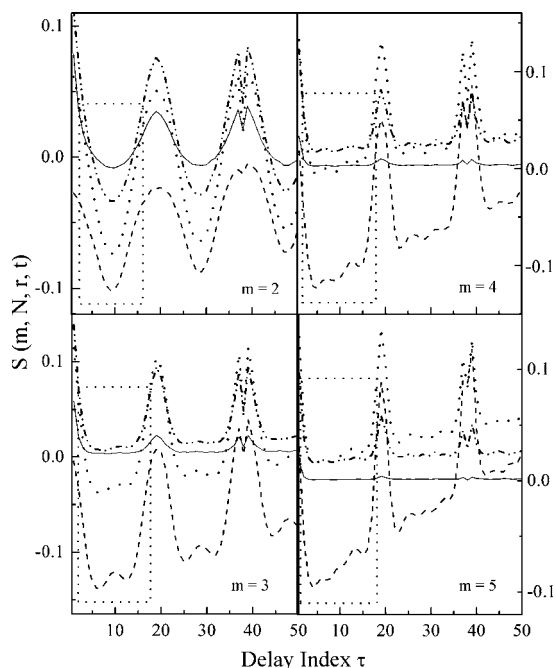


FIG. 2. Determination of time delay using the *C-C* computational method described by Kim *et al.* in Ref. [42]. The statistic $S(m, N, r, \tau)$ is shown on the vertical axis and the lag or delay index τ on the horizontal axis for embedding dimension $m=2, 3, 4$ and 5 , respectively. In each graph, four fixed radius values ($-r=\sigma/2$, $-r=\sigma$, $-r=3\sigma/2$, and $-r=2\sigma$) are used, from half of the standard deviation (σ) of the scalar data to twice the standard deviation, with a half standard deviation increment. The zero crossings and delay values of least variation with r , which are used for averaging a delay index, are shown by the dotted window. This particular set was done on the $I=15$ mA data, and is typical of the computations obtained in this work. The derived delay index is in the range of 4–20 with a corresponding time delay of 8–40 μ s.

least variation with r , which are used for averaging a delay index, are shown by the dotted window. From these computations, the experimental delay index was determined, ranging between 4 and 20 for operating range of discharge currents $I=6-50$ mA. After establishing a “proper” time delay, further computations (such as the correlation dimension) which require this quantity are able to be made next.

IV. EXPERIMENTAL METHODS

A. Glow discharge apparatus

The experiment is performed using a dc glow discharge plasma. The measurement arrangement is shown in Fig. 3. The plasma is sustained inside a glass tube (inner diameter 4.7 cm and 68 cm long). The stainless steel end flanges of the tube are used as the anode and cathode. A 15 k Ω ballast resistor is used in series with a 5 kW power supply (5 kV, 1 A) to limit the current through the discharge. A mechanical plus turbo pump system is used to evacuate the tube to a base pressure of 3×10^{-5} Torr. A high-purity argon gas flow at the rate of 5 SCCM (SCCM denotes cubic centimeters per minute at STP) is maintained with a mass flow controller,

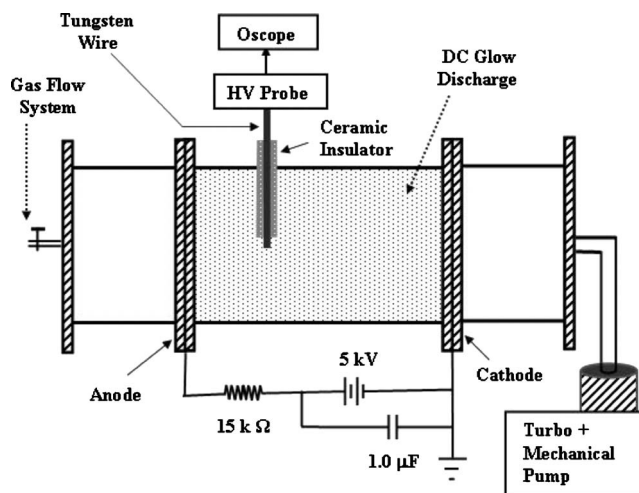


FIG. 3. Experimental setup. A dc glow discharge is sustained between two electrodes with a 15 k Ω ballast resistor to limit the current through the discharge. The main diagnostic used in this work is the high-voltage probe to measure the fluctuations in the plasma floating potentials.

where the pressure is monitored with an absolute pressure (Baratron) manometer. The measurement is performed at a fixed operating pressure $p_0=0.25$ Torr ($p_0r_0=0.59$ Torr cm), and in the range of discharge currents from 0 to 50 mA (current densities from 0 to 28.8 A/m²) with a 1 mA increment.

Single and floating double Langmuir probes are used to measure the plasma parameters. At the fixed pressure level of 0.5 Torr, the electron number density is found to be 2×10^9 cm⁻³ and the electron temperature to be ~ 3.0 eV [43]. A pair of high-voltage probes (Tektronix model P6015A, bandwidth 75 MHz) is deployed to measure the floating potentials and the fluctuations in the floating potentials. From the two-point measurement of the floating potential (two high-voltage probes were separated by 2.6 cm), an average electric field strength of 6.3 V/cm is determined in the argon plasma at 250 mTorr and discharge currents between 0 and 50 mA.

The measurements are performed for fixed glow discharge currents starting from about 5 mA, and stepping upward by 1 mA increments up to 50 mA. For the entire measurement, the high-voltage probe is setup at the center of the positive column plasma. The digitizing fast oscilloscope collects 20 000 data points over an interval of 40 ms at a sampling rate of 500 kHz for each data run.

B. Experimental results

Typical experimental floating potential fluctuations in the glow discharge argon plasma for a fixed gas pressure of 250 mTorr and for several fixed discharge currents is shown in Fig. 4(a). The corresponding Fourier power spectrum is shown on the right in Fig. 4(b). The fluctuations are seen to be random in the range of discharge current $I=6-10$ mA with no major peak frequencies in the corresponding power spectrum. The periodic oscillations are observed for $I=11-20$ mA, which is clearly indicated by the fundamental

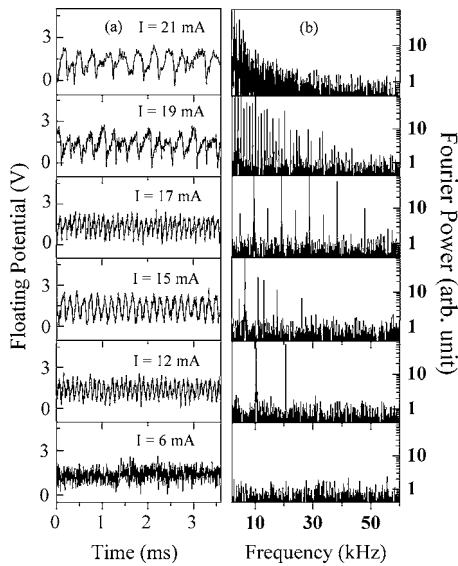


FIG. 4. (a) Sample time evolution (time series) data for the plasma floating potentials at a sampling rate of 500 kHz ($2 \mu\text{s}/\text{point}$) for various fixed discharge currents. The fluctuations look random at 6 mA, periodic between 12 and 19 mA, and chaotic at 21 mA. (b) The corresponding Fourier power spectra are shown with no characteristic peak seen at 6 mA, two peaks at 12 mA, six at 15 mA, nine at 17 mA, and thirty at 19 mA. Finally at 21 mA, the power spectrum yields a broadened spectral structure.

and harmonic peak frequencies in their Fourier spectra. Above $I=20$ mA, the fluctuations become unstable (associated with a broadened spectral structure in the Fourier spectrum).

Here, we attempt to document the shifting modes of behavior as dependent upon the bifurcation parameter (the glow discharge current) for a fixed pressure. We have constructed a skeleton of a bifurcation diagram for our glow discharge system. The power spectrum analyses, a few of which are presented in Fig. 4, have yielded the distinctions which the diagram represents. On the vertical axis of Fig. 5 are the dominant frequencies of each of the periodic data sets (for the data which exhibit clear frequencies in the power spectrum). If the signal is dominated by noise, then the spectrum shows no dominant frequency. If the signal is unstable, showing a broadened spectral structure in the low end of the frequency domain, then the diagram shows a cross-hatched region. As can be seen, aside from some low current values (below $I=11$ mA) where noise seems to dominate, the bifurcations occur rather clearly. Yet, as was pointed out earlier, some small-scale spectral information is lost due to noise contamination of the power spectrum, and so we may only record the distinguishable frequencies. Regardless, these clearly increase in number up to 20 mA, after which the power spectrum no longer shows dominant frequencies, only broadened low-frequency peaks. This is the case until 38 mA, where dominant frequencies emerge again, and so on, as illustrated in the diagram. In fact, beyond the data presented in this study, this behavior continues, the alternating stable and unstable regimes with increasing bifurcation parameter values, indicating parameter dependent intermit-

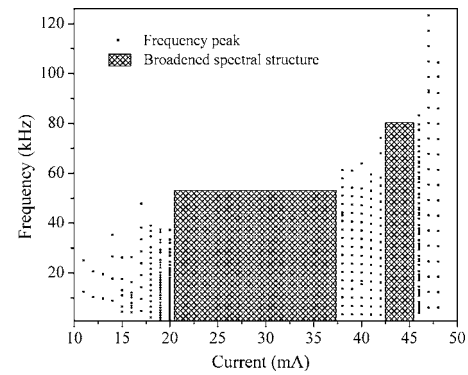


FIG. 5. Distinct frequencies in the Fourier spectrum from Fig. 4 versus discharge current. This graph represents an experimental bifurcation diagram for the discharge plasma. The number of distinct frequencies multiplies as the discharge current is increased. As the current increases to 21 mA, the plasma shows unstable behaviors. For data in a region of instability, a cross-hatched region is shown.

tencies similar to the ones found on the right side of the logistic map's bifurcation diagram in Fig. 1(e). Thus, our experimental glow discharge system exhibits a bifurcation route to instability through frequency multiplication. There were seen two frequencies which were ubiquitous in the data, one near 120 Hz, and the other near 1700 Hz. They induce no harmonics, and seem not to interfere with the other frequencies. These are likely artifacts of some electrical noise; thus they were excluded from the emergent bifurcation frequencies.

Next, we present the results of the correlation dimension computations for the plasma potential fluctuations. In Fig. 6, for the sake of clarity, the derivatives of the correlation integral $d\{\log_{10}[C(r)]\}/d[\log_{10}(r)]$ are shown (versus the logarithm of the embedding space neighborhood radius r) for data from three distinct regions. Figure 6(a) shows 6 mA from the region of random fluctuations, Fig. 6(b) shows 12 mA from periodic oscillations, and Fig. 6(c) shows 21 mA from the unstable region. Figure 7 shows the parameter dependence of the computed correlation dimension on the system's states. In this way, as the bifurcation parameter (discharge current) is changed, one may watch the approximate change in the dimensionality of the attractor. In the low current range (6–10 mA), where the power spectrum suggests that the fluctuations are dominated by random noise, we may cautiously expect the correlation integral to show no scaling region. This is in fact the case [see Fig. 6(a)]. For the periodic range 11–20 mA, conventions would have us expect that the correlation integral would show a scaling region revealing a low integer dimension. Our findings were somewhat consistent with this convention, but as is indicated by the dotted horizontal line in Fig. 6(b), the interpreted dimension shown in Fig. 7 fluctuates around a value of 2 between 11 and 17 mA. This fluctuation of the dimensional estimate could be explained by a number of factors. It could suggest the coexistence of attractors in the data. Since the bifurcation parameter is not perfectly constant, and the behavior of the system may be sensitively dependent upon it, then for a given time series, the data may contain small transient “vis-

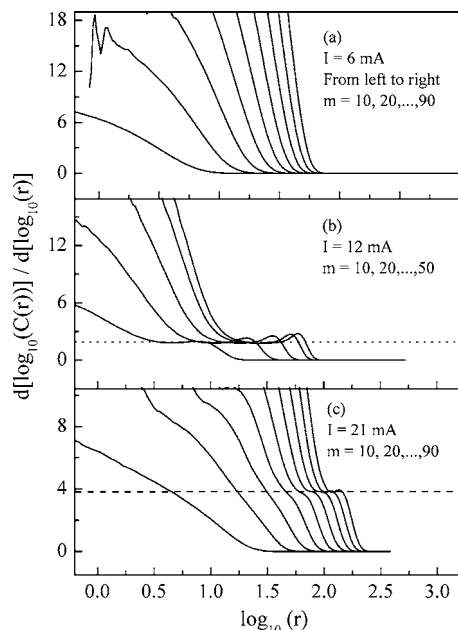


FIG. 6. Computations for the correlation dimension. In (a)–(c), $d[\log_{10}[C(r)]]/d[\log_{10}(r)]$ is plotted versus the logarithm of the embedding space distance r for 6, 12, and 21 mA, respectively. The derivatives of the correlation integrals are examined for any plateau. (a) We recall from Fig. 4 that the data at 6 mA are characterized by random fluctuations, and here no saturating scaling regions are found for all embedding dimensions. Their overall slopes continue to increase with increasing embedding dimension. For visual clarity, computations for embedding dimensions 10 and above are shown. (b) The data set for 12 mA (which showed periodic fluctuations in Fig. 4) shows the plateau from scaling regions (one may clearly see the convergence of the slopes at a value of about 1.8). This saturation occurred robustly at low embedding dimensions (below 50); therefore, higher-dimensional computations were avoided to conserve computation time. (c) This particular data set did not show a scaling region until a relatively high embedding dimension of 30 and above. Here, the convergence of the plateaus (linear slopes) occurs at a value of about 3.8.

its” to a nonperiodic attractor, if one exists. This would potentially skew the interpreted dimension of an otherwise periodic attractor, pulling it away from an integer value, creating a strange nonchaotic attractor [38]. Also, it has been seen that noise in the data will skew the dimension by small amounts, proportional to the amplitude of the noise. We did a simple study of the correlation dimension of a perfect periodic signal (discrete points along a sine wave) with incremental addition of noise. We found that, while the clean sine wave by itself scaled perfectly to a dimension of 1, the successive series, with added noise of increasing amplitude, showed robust scaling at dimension values, which steadily increased with the amplitude of the noise. The dimension increased from a value of 1 for clean data, to a value over 2 for data with noise amplitude which was half the amplitude of the signal.

At $I=18$ mA, the scaling occurs near 3, near 4 at 19 mA, and between 6 and 7 at 20 mA. The existence of strange nonchaotic attractors may be understood not only with re-

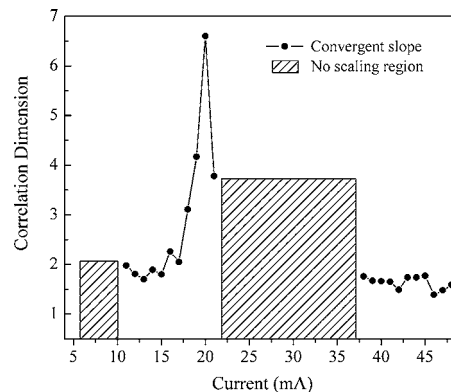


FIG. 7. Estimated correlation dimension for the experimental data and its dependence on the experimental bifurcation parameter (discharge current). All estimations of finite dimensions have a margin of fitting error of 1% in the linear scaling regions. The hatched regions represent data sets whose correlation dimensions did not saturate to a finite value with increased embedding dimensions.

spect to transient intermittency, but can be seen by the bifurcation structure itself. As a system bifurcates, the structure of the attractor also splits in the embedding space. For instance, just before the transition to chaos, pertinent numerical systems bifurcate indefinitely many times as the parameter approaches its critical value. In this state, the attractor assumes a fractal structure, though the dynamics on it are not chaotic. This would yield a noninteger dimension. Also, if the geometry of the parameter space is nontrivial, that is to say, if the periodic region has a complicated boundary separating it from the unstable region, as has been found in numerical parameter spaces [44], then it is possible that within this periodic window, there are some small areas, or islands, of unstable values of the bifurcation parameter. This would serve to skew the dimension of a periodic fluctuation in a way consistent with [38], and perhaps make sense with regard to [44], where such structures are reported to have been found in the parameter space of the Hénon map [45]. For the region after the loss of stability, 21–37 mA, the interpretation of the correlation dimension is very difficult. This region was initially characterized by the presences of broadened spectral structure in the frequency domain. This is an initial suggestion of a chaotic behavior, though not, in itself, a sufficient condition to indicate such. One may then look to the correlation dimension for a noninteger, low-dimensional value. For the first value of 21 mA, a scaling region emerges at a high embedding dimension with a value of approximately 3.8 as indicated by the dashed horizontal line in Fig. 6(c). With the absence of a dominant frequency, and the presence of a noninteger correlation dimension, this is suggestive of deterministic chaos. Beyond this value, the instability is a bit different. There is a broadened spectral structure in the frequency domain, but there is not a clear scaling region on the correlation integral. For many current values in the unstable region, there is a seeming scaling around 12, which fails to ultimately saturate with increased embedding dimension. This has been interpreted in the past [36] as a signature of turbulence in glow discharge systems. It has been pointed out that “almost all systems reach turbulence via chaos” [37].

Perhaps this is the case in our system, but in order to determine precisely the presence of turbulence, a variety of different statistics would need to be applied to the data. This is somewhat beyond the scope of this investigation. Beyond this unstable region, after 37 mA, there is observed regions with a distinct multiple-peak structure in the power spectrum, followed by others which show broadened peak structures. When analyzing the correlation sum for these data, a surprisingly consistent scaling region between 1.4 and 1.8 was located for most of both spectral types as shown in Fig. 7. For the types with broadened spectral structure, there were also seen second scaling regions at higher dimensions, between 4 and 11, but the scaling regions, though distinct, were not robustly linear. We will not disregard this observation, as perhaps it indicates a coexistence of attractors in the data, but the further analysis of it will not be undertaken here. The succession of the distinct spectral regions continues beyond the data presented in this study.

V. DISCUSSION

Based on the results presented above, it is clear that the structure of the parameter space of our system is nontrivial, even if our study was performed on only a cross section of it. For the bifurcation parameter, we have distinguished a period multiplying route to instability, as well as alternating regions of stability and instability. In this way, we can see that the complexity of the parameter space is such that there are multiple transition values of the bifurcation parameter. This has been observed to be the case with many of the numerical bifurcations (for instance, observe the bifurcation diagram of the logistic map in Fig. 1). Though a further examination of the regions of instability would certainly yield a deeper understanding of the chaotic and turbulent phenomena observed, this will have to be undertaken in later studies. The purpose here was to see, in a somewhat high-resolution man-

ner, how the bifurcation behavior of our system looked along the dc current parameter. The hopes were to find the behavior comparable, in some way, to the numerical analogs. This study seems to have shown something quite like this, though there are multiple such bifurcation schemes that numerical and experimental systems tend to exhibit. One driving interest was the findings of surprising complexity in the parameter spaces of seemingly “simple” numerical systems, like the findings of strange parameter space structures in the Hénon map [45].

There are more points of comparison which could potentially be sought between our system and the numerical systems, for instance, finding out whether the locations of successive bifurcation points show the scaling pattern which has been found in numerical systems. Though to do this, we would need higher resolution sets of data. To do this we would need a more precise power supply (as well as perhaps constructing a circuit designed specifically to stabilize the driving current), with which we could distinguish more finely the increments of the current. Future work on this data may include an analysis of the Lyapunov exponents, or Kolmogorov entropies of the data, to distinguish more specifically the nature of the regions of instability. It would also be interesting to attempt multiple cross sections of the parameter space, for different pressure values, to see the geometry of the system in its two-dimensional parameter space.

ACKNOWLEDGMENTS

We would like to thank Diane Porter and Dr. Bill Zhong for accommodating our computational demands, and the late Dr. Eugene Clothiaux of Auburn University for his graciousness in helping us get our laboratory equipped and running. The Plasma Physics Laboratory where this work was done is supported by the DOE Junior Faculty Development Program Grant No. DE-FG02-04ER54792.

-
- [1] M. C. Cross and P. C. Hohenberg, *Rev. Mod. Phys.* **65**, 851 (1993).
 - [2] H. G. Schuster, *Deterministic Chaos: An Introduction* (VCH, New York, 1988).
 - [3] R. F. Ellis and D. N. Arion, *J. Appl. Phys.* **54**, 4895 (1983).
 - [4] W. X. Ding, T. Klinger, and A. Piel, *Phys. Lett. A* **222**, 409 (1996).
 - [5] T. Donahue and G. H. Dieke, *Phys. Rev.* **81**, 248 (1951).
 - [6] R. G. Gibson, *Am. J. Phys.* **51**, 1028 (1983).
 - [7] A. Garscadden, in *Gaseous Electronics*, edited by M. N. Hirsh and H. J. Oskam, (Academic, New York, 1978), Vol. 1, pp. 65–107.
 - [8] M. A. Hassouba, H. I. Al-Naggar, and N. M. Al-Naggar, *Phys. Plasmas* **13**, 073504 (2006).
 - [9] M. Sugawara, K. Murata, T. Ohshima, K. Motohashi, and K. Kobayashi, *J. Phys. D* **14**, L137 (1981).
 - [10] P. S. R. Prasad, R. Singh, and R. K. Thareja, *IEEE Trans. Plasma Sci.* **22**, 224 (1994).
 - [11] J. Qin, L. Wang, D. P. Yuan, P. Gao, and B. Z. Zhang, *Phys. Rev. Lett.* **63**, 163 (1989).
 - [12] F. Greiner, T. Klinger, H. Klostermann, and A. Piel, *Phys. Rev. Lett.* **70**, 3071 (1993).
 - [13] P. Y. Cheung and A. Y. Wong, *Phys. Rev. Lett.* **59**, 551 (1987).
 - [14] R. Timm and A. Piel, *Contrib. Plasma Phys.* **32**, 599 (1992).
 - [15] E. Ott, *Chaos in Dynamical Systems* (Cambridge University Press, Cambridge, U.K., 2002), pp. 23–68.
 - [16] Y. Matsunaga and T. Kato, *J. Phys. Soc. Jpn.* **63**, 4396 (1994).
 - [17] D. D. Sijacic, U. Ebert, and I. Rafatov, *Phys. Rev. E* **70**, 056220 (2004).
 - [18] Y. H. Wang, Y. T. Zhang, D. Z. Wang, and M. G. Kong, *Appl. Phys. Lett.* **90**, 071501 (2007).
 - [19] Ding Weixing, Huang Wei, Wang Xiaodong, and C. X. Yu, *Phys. Rev. Lett.* **70**, 170 (1993).
 - [20] N. Ohno, A. Komori, M. Kono, and Y. Kawai, *Phys. Fluids B* **5**, 796 (1993).
 - [21] Y. T. Zhang, D. Z. Wang, and M. G. Kong, *J. Appl. Phys.* **100**, 063304 (2006).
 - [22] P. Y. Cheung, S. Donovan, and A. Y. Wong, *Phys. Rev. Lett.*

- 61**, 1360 (1988).
- [23] B. Bruhn, *Phys. Plasmas* **11**, 4446 (2004).
- [24] P. Jonas, B. Bruhn, B.-P. Koch, and A. Dinklage, *Phys. Plasmas* **7**, 729 (2000).
- [25] B. Bruhn, B.-P. Koch, and P. Jonas, *Phys. Rev. E* **58**, 3793 (1998).
- [26] F. Takens, in *Dynamical systems and turbulence*, edited by D. A. Rand and L.-S. Young, *Lecture Notes in Mathematics* Vol. 898 (Springer-Verlag, Berlin, 1981), pp. 366-381.
- [27] D. Ruelle and F. Takens, *Commun. Math. Phys.* **20**, 167 (1971).
- [28] J. D. Farmer and J. J. Sidorowich, *Phys. Rev. Lett.* **59**, 845 (1987).
- [29] N. H. Packard, J. P. Crutchfield, J. D. Farmer, and R. S. Shaw, *Phys. Rev. Lett.* **45**, 712 (1980).
- [30] A. Atipo, G. Bonhomme, and T. Pierre, *Eur. Phys. J. D* **19**, 79 (2002).
- [31] R. M. May, *Nature (London)* **261**, 459 (1976).
- [32] http://en.wikipedia.org/wiki/Image:LogisticMap_BifurcationDiagram.png
- [33] H. Kantz and T. Schreiber, *Nonlinear Time Series Analysis* (Cambridge University Press, Cambridge, U.K., 1997), pp. 20-70.
- [34] P. Grassberger and I. Procaccia, *Physica D* **9**, 189 (1983); *Phys. Rev. Lett.* **50**, 346 (1983).
- [35] M. B. Kennel, R. Brown, and H. D. I. Abarbanel, *Phys. Rev. A* **45**, 3403 (1992).
- [36] M. Koga and Y. Kawai, *Phys. Plasmas* **10**, 650 (2003).
- [37] T. Fukuyama, K. Taniguchi, and Y. Kawai, *Phys. Plasmas* **9**, 1570 (2002).
- [38] X. Wang, M. Zhan, C. Lai, and Y. Lai, *Phys. Rev. Lett.* **92**, 074102 (2004).
- [39] W. X. Ding, H. Deutsch, A. Dinklage, and C. Wilke, *Phys. Rev. E* **55**, 3769 (1997).
- [40] W. Liebert and H. G. Schuster, *Phys. Lett. A* **142**, 107 (1989).
- [41] A. M. Fraser and H. L. Swinney, *Phys. Rev. A* **33**, 1134 (1986).
- [42] H. S. Kim, R. Eykholt, and J. D. Salas, *Physica D* **127**, 48 (1999).
- [43] N. K. Podder, A. V. Tarasova, and R. B. Wilson IV, *IEEE Trans. Plasma Sci.* **35**, 1034 (2007).
- [44] J. A. C. Gallas, *Phys. Rev. Lett.* **70**, 2714 (1993).
- [45] M. Hénon, *Commun. Math. Phys.* **50**, 69 (1976).